Medical Engineering & Physics xxx (2012) xxx–xxx

Contents lists available at SciVerse ScienceDirect

Medical Engineering & Physics

journal homepage: www.elsevier.com/locate/medengphy

A computer-aided diagnosis approach for emphysema recognition in chest radiography

Giuseppe Coppini[a,*], Massimo Miniati[b], Simonetta Monti[a], Marco Paterni[a], Riccardo Favilla[a], Ezio Maria Ferdeghini[a]

[a] CNR Institute of Clinical Physiology, Pisa, Italy
[b] Department of Medical and Surgical Critical Care, University of Florence, Italy

ARTICLE INFO

Article history:
Received 6 June 2011
Received in revised form 15 February 2012
Accepted 21 March 2012

Keywords:
Chest radiography
Emphysema
Computer-aided-diagnosis (CAD) systems
Neural networks
Lung segmentation

ABSTRACT

The purpose of this work is twofold: (i) to develop a CAD system for the assessment of emphysema by digital chest radiography and (ii) to test it against CT imaging. The system is based on the analysis of the shape of lung silhouette as imaged in standard chest examination. Postero-anterior and lateral views are processed to extract the contours of the lung fields automatically. Subsequently, the shape of lung silhouettes is described by polyline approximation and the computed feature-set processed by a neural network to estimate the probability of emphysema.

Images of radiographic studies from 225 patients were collected and properly annotated to build an experimental dataset named EMPH. Each patient had undergone a standard two-views chest radiography and CT for diagnostic purposes. In addition, the images (247) from JSRT dataset were used to evaluate lung segmentation in postero-anterior view.

System performances were assessed by: (i) analyzing the quality of the automatic segmentation of the lung silhouette against manual tracing and (ii) measuring the capabilities of emphysema recognition. As to step i, on JSRT dataset, we obtained overlap percentage (Ω) $92.7 \pm 3.3\%$, Dice Similarity Coefficient (DSC) $95.5 \pm 3.7\%$ and average contour distance (ACD) 1.73 ± 0.87 mm. On EMPH dataset we had $\Omega = 93.1 \pm 2.9\%$, DSC = $96.1 \pm 3.5\%$ and ACD = 1.62 ± 0.92 mm, for the postero-anterior view, while we had $\Omega = 94.5 \pm 4.6\%$, DSC = $91.0 \pm 6.3\%$ and ACD = 2.22 ± 0.86 mm, for the lateral view. As to step ii, accuracy of emphysema recognition was 95.4%, with sensitivity and specificity 94.5% and 96.1% respectively. According to experimental results our system allows reliable and inexpensive recognition of emphysema on digital chest radiography.

1. Introduction

Emphysema is a structural abnormality of the lung and its recognition is based on tests that reflect lung structure rather than function [1,2]. Computed tomography (CT) is currently the most accurate imaging technique for diagnosing emphysema in vivo [3]; different quantitative methods to assess emphysema by CT have been proposed, all of them being based on densitometric image features [4]. Extensive use of CT technique to assess emphysema seems, however, unwarranted due to the high cost and substantial radiation burden to the patient.

Chest radiography has long been used in clinical practice for the evaluation of emphysema [5,2]. Radiographic abnormalities suggestive of emphysema are of two types: those related to hyperinflation (depression and flattening of the diaphragmatic contours, increased retrosternal space, the latter being observed in lateral view only), and those related to the distribution of destructive lesions and concomitant changes in the vascular pattern [5]. Recognition of the latter changes is difficult and often results in large inter-observer variability. Conversely, signs of lung hyperinflation are more easily detectable even by less experienced physicians using standard two-view (postero-anterior and lateral) radiography. It is also worth noting that chest radiography would represent a far less expensive diagnostic tool than CT, and entails a much lower effective radiation dose [6].

Recently, the value of chest radiography to detect pulmonary emphysema was reappraised using CT as the reference diagnostic standard [7], confirming its diagnostic accuracy. In addition, computational approaches to the use of digital chest radiography for emphysema detection were explored [8]. Quantitative shape descriptors of hand traced pulmonary silhouettes proved quite accurate in such tasks [9]. Sensitivity and specificity of two different sets of shape features designed to recognize emphysema were studied. A polyline shape description applied to standard two-sided

* Corresponding author. Tel.: +39 0503153480; fax: +39 0503152166.
E-mail address: coppini@ifc.cnr.it (G. Coppini).

1350-4533/$ – see front matter © 2012 IPEM. Published by Elsevier Ltd. All rights reserved.
http://dx.doi.org/10.1016/j.medengphy.2012.03.011

chest radiographs, yielded an accuracy of about 90.3%, a sensitivity of 88.3%, and a specificity 90.7%. More recently those findings were confirmed against CT imaging [10]. On these bases, automatic procedures to assist emphysema diagnosis in clinical routine could be designed according to a simple computational framework including segmentation of lung silhouettes in two-view radiography and analysis of their shape.

Segmentation of lung fields in postero-anterior chest radiographs has long been studied according to different approaches. They include rule-based schemes [11–16], methods based on pixel classification [17–20], hybrid approaches [21], active shape models (ASM) and active appearance models (AAM) [22–24]. A comparison of several segmentation methods is provided by van Ginneken et al. [23] using the images form JSRT dataset [25]. In particular, their findings support the versatility and flexibility of supervised approaches in segmenting lung fields in postero-anterior views. The best results were achieved by pixel classification or by combining pixel classification with model based methods. These results suggest that accurate segmentation can be achieved by properly integrating prior anatomical knowledge with prototypical image appearance. In addition, it stands to reason that trainable models can ensure performances comparable to human observers.

Unfortunately, segmentation of lung profile in lateral views is scarcely documented in the literature [26,27]. On the other hand, lateral projection provides important diagnostic information for recognizing emphysema: expansion of the retrosternal space is appreciated only in the lateral view which also accurately describes diaphragm flattening [8]. It must be pointed out that, due to the thickness of the imaged object and the overlapping of the lung fields, lateral views usually exhibit inferior image quality, both in terms of contrast and in terms of signal-to-noise ratio. Therefore, tracing the lung silhouette in lateral chest projections needs robust computational methods able to efficiently match high-level knowledge and local image features.

To face the problem of lung field segmentation in both postero-anterior and lateral view, we modeled the lung boundary as a closed fuzzy-curve. Such a model is quite general and able to cope with uncertainty due to poor image quality. In so doing, the segmentation task is referred back to estimating the associated membership. The latter is expected to be non-linearly and space-varying dependent on image features. Multilayer neural networks are well known universal approximators, and, in addition, are expected to provide good generalization capabilities [29]. We used multilayer neural networks to learn fuzzy memberships from differential image features. According to our model, lung boundary is defuzzified exploiting the relaxation of a modified Kohonen network. Due to its topology-preserving property, this neural network acts as a ridge detector able to smoothly enforce boundary closure.

The shape of automatically segmented lung fields was analyzed using a polyline descriptor we have preliminary tested on hand-traced lung fields [10]. Emphysema probability is estimated by a neural network trained using CT output. The behavior of the system was also examined in the presence of skeletal distortions. To develop and test our system we utilized the datasets described in Section 2. In Section 3, we explain both the method for lung segmentation in two-view radiography, and the shape analysis/classification phases. Implementation details and testing results are given in Sections 4 and 5.

2. Clinical dataset

Standard chest radiographs of 225 subjects were used to develop and test the automated diagnostic tool. All patients underwent postero-anterior and lateral digital chest radiographs and CT (within a week from the radiographic study) for diagnostic purposes. To ensure privacy and blind evaluation by medical observers, the whole set of chest radiographs were fully anonymized. For convenience, this radiographic dataset was named EMPH. One hundred forty-one patients in EMPH had a firm clinical diagnosis of stable COPD and 84 were age- and sex-matched (smokers, or former smokers) with normal lung function. Radiographic projections (Thorax 2000, IMIX, Finland) were obtained at a standard 2-m focus-to-detector distance with the patients upright, holding their breath at full inspiration. Each radiograph was 2000×2000 pixels (198 μm per pixel), with a dynamic range of 12 bits. Images were obtained by the radiographic equipment in standard operational conditions, and no further post-processing was applied. To develop and test the system, an expert physician (not aware of the patients diagnosis) was asked to interactively trace the lung field boundaries. For each image, the observer located a small set of key points (typically about 20 knots). The contour of the lung areas was drawn by interpolating the knots with cubic splines.

Using CT images, the severity of emphysema was scored on a nonparametric scale from 0 (no emphysema) to 100 by the panel grading (PG) method of Thurlbeck et al. [3]. This consists of 16 inflation-fixed, paper-mounted, midsagittal whole lung sections that are arranged at intervals of 5 between 0 and 50, and at intervals of 10 between 60 and 100. A score of 5 or less is consistent with trace emphysema, a score of 10–30 indicates mild emphysema, a score 30–50 moderate emphysema, and a score 50–100 severe emphysema. CT scans were reconstructed in the axial, sagittal and coronal planes. In scoring emphysema, two independent raters examined sagittal lung sections, and gave them the score of the standard most closely similar, or a score between two standards. The two raters were blinded to clinical and chest radiography data. The PG scores by the two raters were averaged. Ninety-two patients resulted to have emphysema (PG score >0).

To build and test the system, patients were randomly arranged in two groups, $EMPH_1$ ($N = 113$) and $EMPH_2$ ($N = 112$), an equal number (46) of emphysema cases at CT being included in both subsets.

To the unique purpose of evaluating the segmentation capabilities of our method, we also used the images from JSRT dataset [25] including 247 postero-anterior radiographs (matrix size 2048×2048, 175 μm per pixel and 12 bit of density resolution) available at JSRT web site (http://www.jsrt.or.jp). This dataset was originally designed to test lung nodule recognition methods, reference lung boundaries [23] (SCR database) are made available at http://www.isi.uu.nl. JSRT images were grouped in two folds $JSRT_1$ and $JSRT_2$ containing 124 and 123 images respectively. It is worth mentioning that, being JSRT images obtained digitizing conventional film radiographies, images have different contrast as compared to digital chest images.

3. Method

The developed system implements the following phases:

1. Segmentation of lung fields,
2. Description of lung shape,
3. Estimation of emphysema probability.

3.1. Segmentation of lung fields

The lung boundary is modeled as a closed fuzzy-curve that is defined by assigning its membership function. As we said in the Introduction, segmentation is reduced to the identification of fuzzy-membership from image features. To this end, we build a neural network architecture including both supervised and

Please cite this article in press as: Coppini G, et al. A computer-aided diagnosis approach for emphysema recognition in chest radiography. Med Eng Phys (2012), http://dx.doi.org/10.1016/j.medengphy.2012.03.011

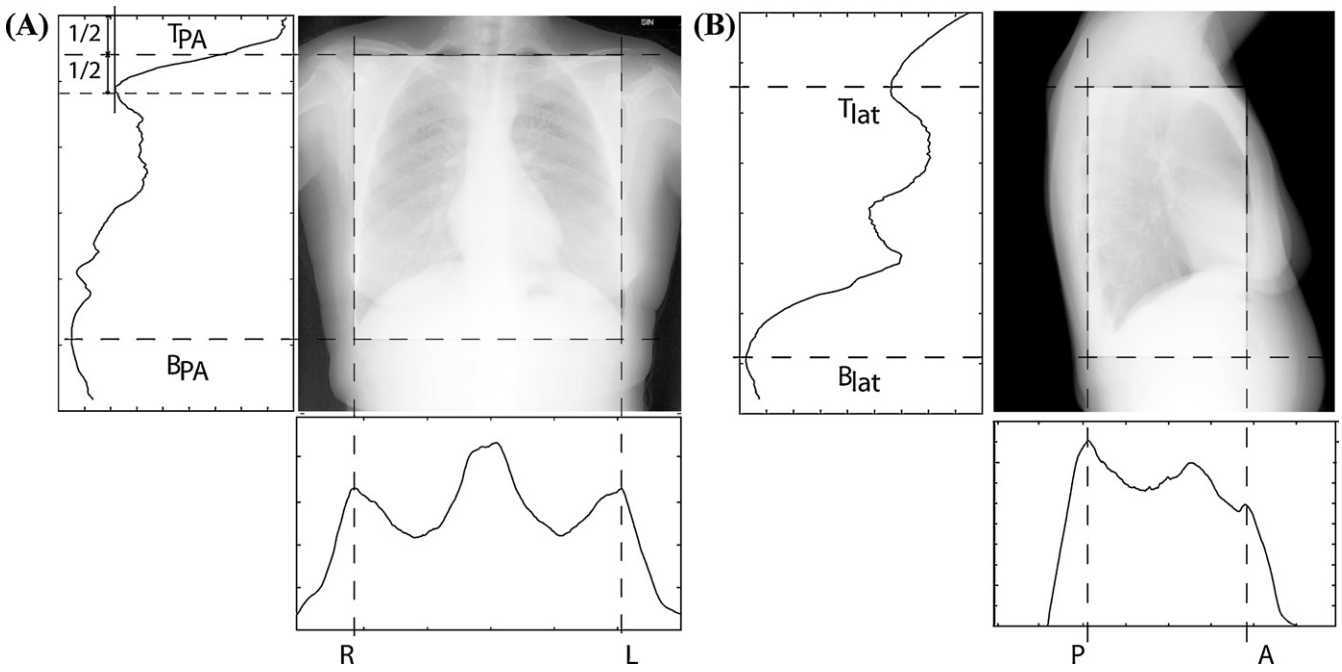

Fig. 1. Lung fields bounding box computation: (A) postero-anterior view and (B) lateral view.

unsupervised neural networks. As detailed in the following subsections, three dedicated networks were designed to estimate the fuzzy membership of right and left lung fields in postero-anterior view and the global lung field in lateral view. To enforce approximate translation and scale invariance and optimize the use of prior knowledge, for each patient, image plane coordinates were normalized. In particular, lung fields were re-centered and the scale of each coordinate axis was adapted to the varying size of lung silhouette. Once the membership function is computed, lung boundary is found by a self-organizing network adapted from Kohonen map [28] and able to act as a ridge detector able to enforce boundary closure.

using the horizontal and vertical gray-level profiles an approximate bounding-box of the lung fields is identified as follows:

1. Postero-anterior view. Left L and right R margins are located by the rightmost and leftmost local maxima of the horizontal profile respectively. Top margin T_{PA} and bottom margin B_{PA} are identified in the vertical profile: T is given by the point set midway between top border of the image and the position of the top peak; B is located as the bottom peak.
2. Lateral view. Anterior A and posterior P margins are identified in the horizontal profile by the posterior and anterior gray level peak, respectively. The top T_{lat} and bottom B_{lat} margin are set in the vertical profile as the top and bottom peaks.

3.1.1. Normalization of position and scales of image reference

The aim of this step is the achievement of (approximate) invariance against image centering and scaling. As shown in Fig. 1, In each image, new coordinates (x, y) are introduced from the original $(\hat{x}, \hat{y})$ by setting the new origin at the top left corner (x_{TLC}, y_{TLC}) of the bounding-box, and normalizing the scale of each axis by the

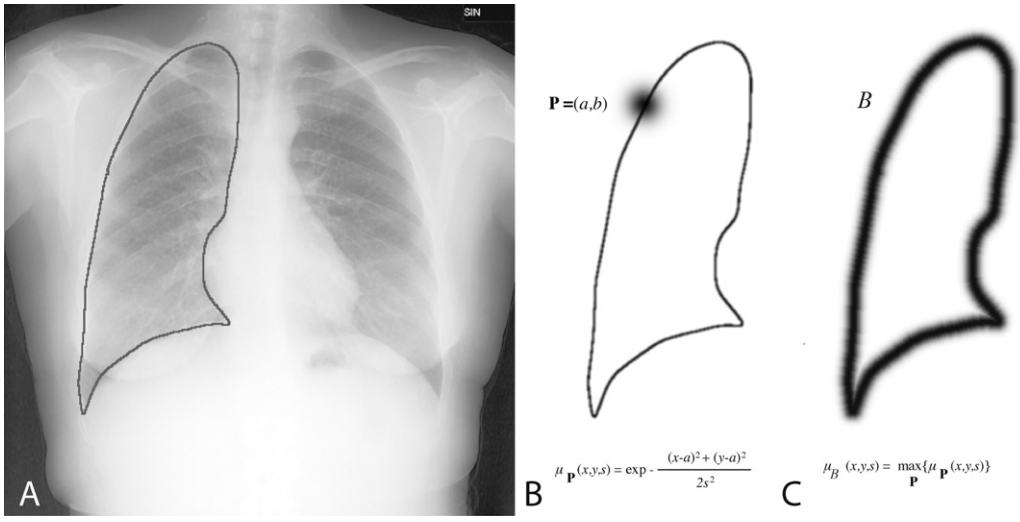

Fig. 2. (A) Hand traced lung boundary and (B and C) its fuzzy representation: (B) fuzzy membership of point P, (C) the fuzzy membership of the entire curve.

Please cite this article in press as: Coppini G, et al. A computer-aided diagnosis approach for emphysema recognition in chest radiography. Med Eng Phys (2012), http://dx.doi.org/10.1016/j.medengphy.2012.03.011

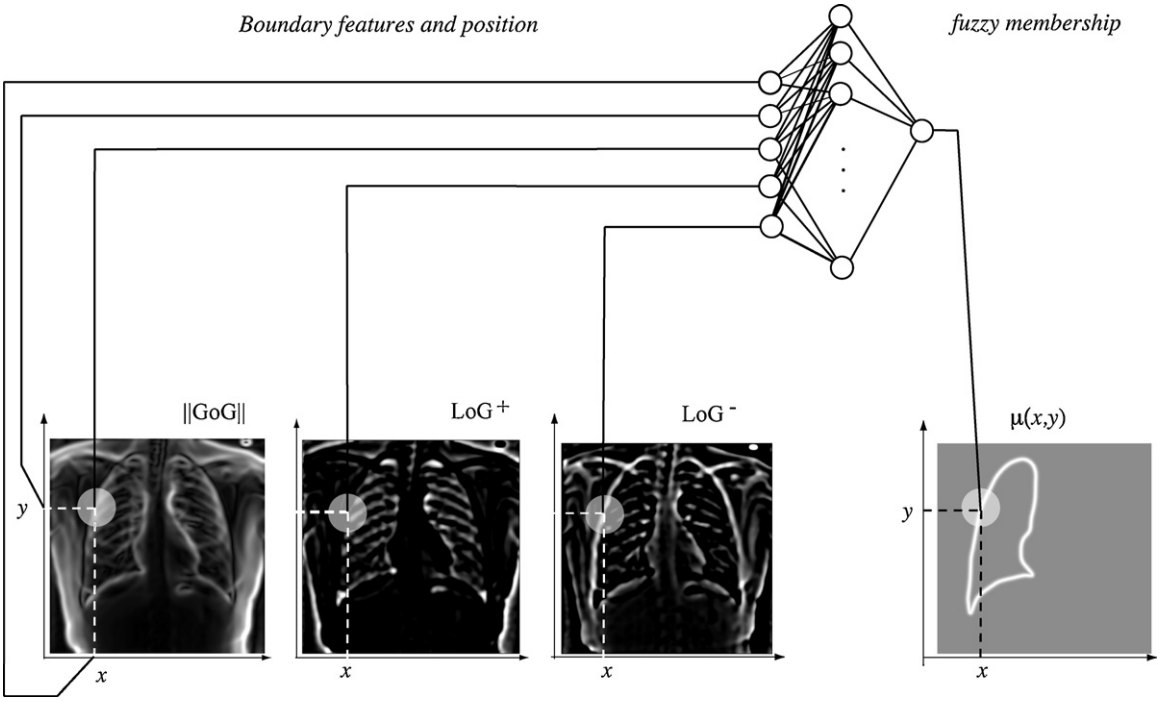

Fig. 3. Estimation of the membership function from image features.

length of the corresponding side of the bounding-box (w, h respectively). The transformation between the two frames is given by the equation:

$$x = \frac{1}{w}(\hat{x} - \hat{x}_{TLC})$$
$$y = \frac{1}{h}(\hat{y} - \hat{y}_{TLC}) \quad (1)$$

3.1.2. Fuzzy representation of lung boundary

The lung contour is a closed curve represented in parametric form as $\mathbf{r}(s) = (x(s), y(s))$, where s is a convenient parameter. The set B of the points in $\mathbf{r}(s)$ is an ordinary (crisp) point set. To account for the fuzziness of the boundary the s neighborhood of the point $\mathbf{P} = (a, b)$ is defined as the fuzzy set $\mathcal{I}_{\mathbf{P}} = \{\mu_{\mathbf{P}}(x, y, s)|(x, y)\}$ of points (x, y) in the image plane having the normalized membership function with Gaussian profile:

$$\mu_{\mathbf{P}}(x, y, s) = \exp^{-((x-a)^2+(y-b)^2)/(2s^2)} \quad (2)$$

The fuzzy union of all s neighborhoods of the points $\mathbf{P} \in B$ is defined as the fuzzy representation R of the boundary:

$$B = \bigcup_{\mathbf{P}} \mathcal{I}_{\mathbf{P}} \quad (3)$$

the membership function $\mu_B(x, y, s)$ of B being defined by the equation:

$$\mu_B(x, y, s) = \max_{\mathbf{P}}\{\mu_{\mathbf{P}}(x, y, s)\}. \quad (4)$$

As depicted in Fig. 2c, a *fuzzy* strip is centered on the traced boundary. The width of the strip is controlled by the s parameter. The original contour B can be retrieved by locating the ridge of μ. The adopted defuzzification method is described in detail in Section 3.1.3.

Computation of $\mu_B(x, y, s)$ from image features was based on the following considerations. In chest radiography, gray levels result from the combined attenuation of the different tissues along a projection ray. Consequently, absolute gray values are not well suited to individuate single physical objects and, in general, they are not adequate to locate boundaries. On the other hand, the application of differential operators, which are sensitive to local spatial changes of grays, is expected to provide significant information about the lung silhouette [17]. In this view, image gradient and Laplacian are largely employed in standard edge-detection methods and were selected as low-level features to estimate $\mu_B(x, y, s)$. Gradient intensity estimates the edge strength, gradient ridges being possible edge locations. Similarly, zero-crossings of Laplacian are possible edges. The latter property can be exploited by processing the positive and negative parts of Laplacian separately. Therefore, the following differential operators were utilized (Fig. 3):

1. The magnitude of gradient $|\nabla I(x, y)|$ that was estimated by Gradient of Gaussian GoG_σ:

$$\|\nabla I(x, y)\| \approx \|GoG_\sigma(x, y)\| = \left[\left(\frac{\partial G_\sigma(x, y)}{\partial x} \otimes I(x, y)\right)^2 + \left(\frac{\partial G_\sigma(x, y)}{\partial y} \otimes I(x, y)\right)^2\right]^{1/2} \quad (5)$$

2. The positive and negative parts of the Laplacian $\nabla^2 I(x, y)$. The latter was computed by Laplacian of Gaussian, LoG_σ:

$$\nabla^2 I(x, y) \approx \mathrm{LoG}_\sigma(x, y) = \frac{\partial^2 G_\sigma(x, y)}{\partial x^2} \otimes I(x, y) + \frac{\partial^2 G_\sigma(x, y)}{\partial y^2} \otimes I(x, y), \quad (6)$$

positive and negative parts were obtained as:

$$\mathrm{LoG}_\sigma^+(x, y) = \max(\mathrm{LoG}_\sigma(x, y), 0)$$
$$\mathrm{LoG}_\sigma^-(x, y) = \max(-\mathrm{LoG}_\sigma(x, y), 0). \quad (7)$$

The next step toward lung segmentation was the computation of a proper mapping:

$$\mathcal{M}(\|\mathrm{GoG}_\sigma\|, \mathrm{LoG}_\sigma{}^+, \mathrm{LoG}_\sigma{}^-) \mapsto \mu_B(x, y, s)$$

Please cite this article in press as: Coppini G, et al. A computer-aided diagnosis approach for emphysema recognition in chest radiography. Med Eng Phys (2012), http://dx.doi.org/10.1016/j.medengphy.2012.03.011

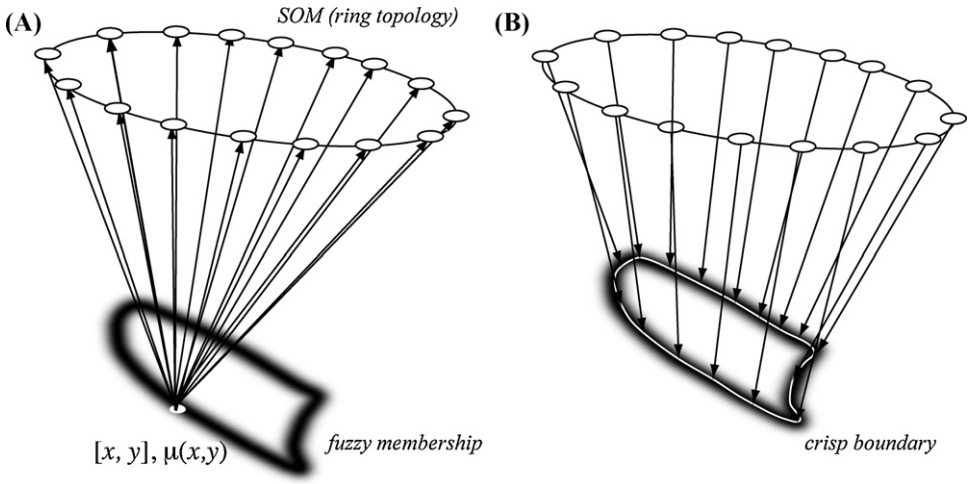

Fig. 4. Topology of the SOM for boundary defuzzification.

utilizing the available prior knowledge about lung silhouette appearance as traced by experts. To this aim, a feed-forward neural network was utilized. The input to the network were the coordinates (x, y) and a corresponding image features $\|\mathrm{GoG}_\sigma(x, y)\|$, $\mathrm{LoG}_\sigma{}^+(x, y)$, $\mathrm{LoG}_\sigma{}^+(x, y)$. The value o of the (single) output unit was the desired membership function at (x, y).

Such a network tends to learn the average conditional target given the input feature vector [29] so that:

$$o(x, y, \|\mathrm{GoG}_\sigma\|, \mathrm{LoG}_\sigma{}^+, \mathrm{LoG}_\sigma{}^-) = \langle \mu_B(x, y, s) | (x, y, \|\mathrm{GoG}_\sigma\|, \mathrm{LoG}_\sigma{}^+, \mathrm{LoG}_\sigma{}^-) \rangle \quad (8)$$

and behaves as a space-varying non-linear operator according to the mapping provided by the training samples.

3.1.3. Boundary defuzzification

The crisp boundary is found by exploiting the relaxation of a Self Organizing Map (SOM) [28]. Let $\mathcal{M}$ be a SOM network composed by a number L of units arranged according to a ring topology as shown in Fig. 4. At a given time t, each unit processes the coordinates (x, y) of a randomly chosen point P: the ith unit has two adaptable connections: $\mathbf{w}_i = (w_{i1}, w_{i2})$. The ordinary weight update rule of SOM is as follows:

$$\Delta \mathbf{w}_i = \alpha(t) \Lambda(i, j, t)(\mathbf{x}_j - \mathbf{w}_i) \quad (9)$$

where i is the winning unit on input j, that is:

$$i = \underset{k}{\operatorname{argmin}} \|\mathbf{x}_j - \mathbf{w}_k\| \quad (10)$$

According to Kohonen [28], $\alpha(t)$ is a gain function that decreases linearly with t and $\Lambda(i, j, t)$ is a neighborhood function whose support decreases linearly with t. Unfortunately, this equation produces a set of weights that covers the entire image plane. On the other hand, membership function values are not considered in Eq. (9). Consequently, to locate a connected closed path corresponding to the ridge of the membership function μ, Eq. (9) goes to incorporate $\mu(x, y)$ by applying the updating rule:

$$\Delta \mathbf{w}_i = \alpha(t) \Lambda(i, j, t) \mu(x, y)(\mathbf{x}_j - \mathbf{w}_i) \quad (11)$$

In this way, weights tend to move toward image points with a large membership values, eventually stopping at its ridge. In facts, weights are changed if and only if $\mu(x, y) \neq 0$. Moreover, when $\mu(x, y)$ is small weight change tends to be negligible, while for larger values of $\mu(x, y)$ (e.g., nearby ridges) weight change is more pronounced.

3.2. Description of lung shape

Lung shape alterations due to emphysema can be characterized by a limited set of numerical features [8]. The adopted shape descriptor is obtained by a polygonal approximation of the lung boundary. The lung shape descriptor was designed to ensure high sensitivity and specificity. Particular attention was paid to cope with shape anomalies related to skeletal distortions rather than to emphysematous process.

As shown in Fig. 5, four points are identified in the postero-anterior view corresponding to the apex and the costophrenic angle of the right and left lung, respectively (these are identified in Fig. 5a as A_R, A_L, C_R, C_L respectively). In the lateral view, the four points are the costophrenic angle posteriorly, the cardiophrenic angle anteriorly, the lung apex, and the maximum vertical distance of the perpendicular drawn from the line joining the costophrenic to the cardiophrenic angle (labeled in Fig. 5b as A_T, P_T, C_A, C_P). The points identified on each radiograph are the corners of a quadrilateral having area A_T.

Next, on each radiograph, the program identifies three triangles each having the base on a side of the quadrilateral and the height equal to the maximum vertical distance from the base to the superjacent lung segment (Fig. 5). Each triangle is described by three numerical features: (i) normalized area $a_n = a/(A_T)$, or the ratio of the triangle area a to the total area A_T; (ii) height ratio $h_r = h/b$, or the ratio of the triangle height h to the triangle base b; (iii) base ratio $b_r = c/b$, or the projection of the triangle minor side c on the triangle base b divided by the base length.

In emphysematous lungs, the normalized area of the triangle below the diaphragms is expected to decrease due to the depression and flattening of the diaphragmatic contours associated with chronic hyperinflation. Conversely, the normalized area of the triangles under the costal and retrosternal sides of the lungs is expected to increase. The height ratio is a numerical index of the maximum bending of a given anatomic segment of the lung, and the base ratio indicates the position, along the triangle base, where the maximum bending occurs. At the end of the procedure, the shape vector from each radiograph includes nine numerical features describing the lung shape.

3.3. Estimate of emphysema probability

The probability p of emphysema is estimated by a dedicated neural network. It is fed by the two shape vectors computed from each radiographic view, and is trained to output the estimated p.

Please cite this article in press as: Coppini G, et al. A computer-aided diagnosis approach for emphysema recognition in chest radiography. Med Eng Phys (2012), http://dx.doi.org/10.1016/j.medengphy.2012.03.011

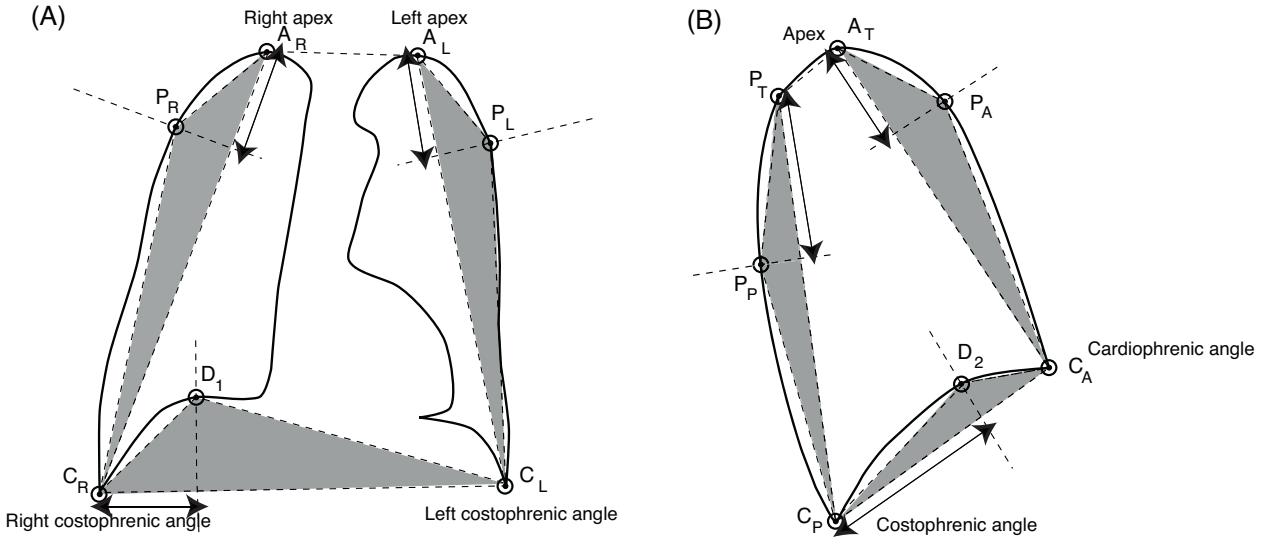

Fig. 5. Shape description: reference points for polyline approximation for (A) postero-anterior view and (B) lateral view.

Network topology and training is detailed in Section 4.2. Once a probability cut-off p_{TH} is set, each case is classified according to the rule:

$p \geq p_{TH}$ class is emphysema
$p < p_{TH}$ class is non-emphysema

4. Implementation

A software application was built to implement the described system. As to system parameter tuning and neural network training the following procedures were applied.

4.1. Training segmentation networks

A. EMPH dataset. Three neural networks were designed: two of them were dedicated to the postero-anterior view to estimate the fuzzy membership of right and left lung respectively, while the third network was trained to estimate the overall lung silhouette in the lateral view. Fuzzy boundaries for training were obtained by applying Eq. (4) to the contours traced by physicians on the dataset images (to define the support of fuzzy membership we set $s = 3$ mm). Images were down-sampled (following Gaussian smoothing) to a matrix 256×256. For each image the module of $\mathrm{GoG}_\sigma(x, y)$ and the $\mathrm{LoG}_\sigma(x, y)$ were computed using $\sigma = 4.0$ mm. Afterwards, from each projection 2000 points were randomly extracted satisfying the constraint that a half of them lied in the support (set at $6 \times s = 18$ mm of the μ_B function) of the teaching fuzzy boundary. For each point (x, y) the input pattern was $[x, y, \| \mathrm{GoG}_\sigma \|, \mathrm{LoG}_\sigma{}^+, \mathrm{LoG}_\sigma{}^-]$, while the teaching output was $\mu_B(x, y, s)$.

Feed-forward networks with one hidden layer were used. The network segmenting postero-anterior views had 5 input units, 20 hidden unit and one output unit, the network for lateral views had 5 input unit, 25 hidden units and one output unit. Network topology was selected by varying the number of hidden units from a minimum of 5 to a maximum of 50 and selecting the best performing architecture. Hidden units had a logistic activation function while output units had linear activation. Training was performed by error back-propagation rule with adaptive learning rate [29]. For each network, the training was firstly done by using the images in EMPH_1 and testing the results on EMPH_2. One tenth (15 cases) of the images in the training set was kept apart and used only to evaluate the generalization error during weight adaption procedure. Training was stopped after the generalization error ceased to decrease. In any case, a maximum number of 5×10^5 training epochs was imposed. To reduce the risk of being trapped in unfavorable local minima of the error function, ten training sessions with different randomly initialized weights were performed. The network with the lowest generalization error was retained. Training was then repeated by interchanging the roles of EMPH_1 and EMPH_2.

B. JSRT dataset. In this case, we trained only the two networks designed for the postero-anterior view, while keeping the same topology and training procedure adopted for the EMPH dataset. Similarly to the case of EMPH dataset, JSRT_1 was firstly used as a training set and JSRT_2 as a test set. Training was repeated interchanging training and test sets.

4.2. Training emphysema probability network

We used a multilayer network having 18 input units, two hidden layers with 15 and 10 units respectively and a single output unit. Hidden units had a sigmoidal activation while the output unit had linear activation. Output is trained to estimate emphysema probability given the input shape features. Teaching output was set to 0 for non-emphysema, and to 1 for emphysema. The network was trained by error back-propagation with adaptive learning rate. All the cases in EMPH dataset were used for training by the leave-one-out method [29]. Training of emphysema probability network was performed using (separately) shape features from (a) manual segmentation and (b) automatic segmentation.

5. Results

Specific tests were performed to evaluate the efficiency and effectiveness of both the segmentation and the shape classification processes. The execution time of the overall procedure, including postero-anterior and lateral lung segmentation, shape analysis and classification, is about 4.5 ± 0.7 s on a iMAC computer equipped with 2.4 GHz Intel Core 2 Duo processor (4 GB RAM), no particular optimization being applied. Though several improvements are possible, e.g., segmentation of different lung profiles can be parallelized by exploiting multicore processors, computation time looks well suited for clinical application (Figs. 6–8).

Please cite this article in press as: Coppini G, et al. A computer-aided diagnosis approach for emphysema recognition in chest radiography. Med Eng Phys (2012), http://dx.doi.org/10.1016/j.medengphy.2012.03.011

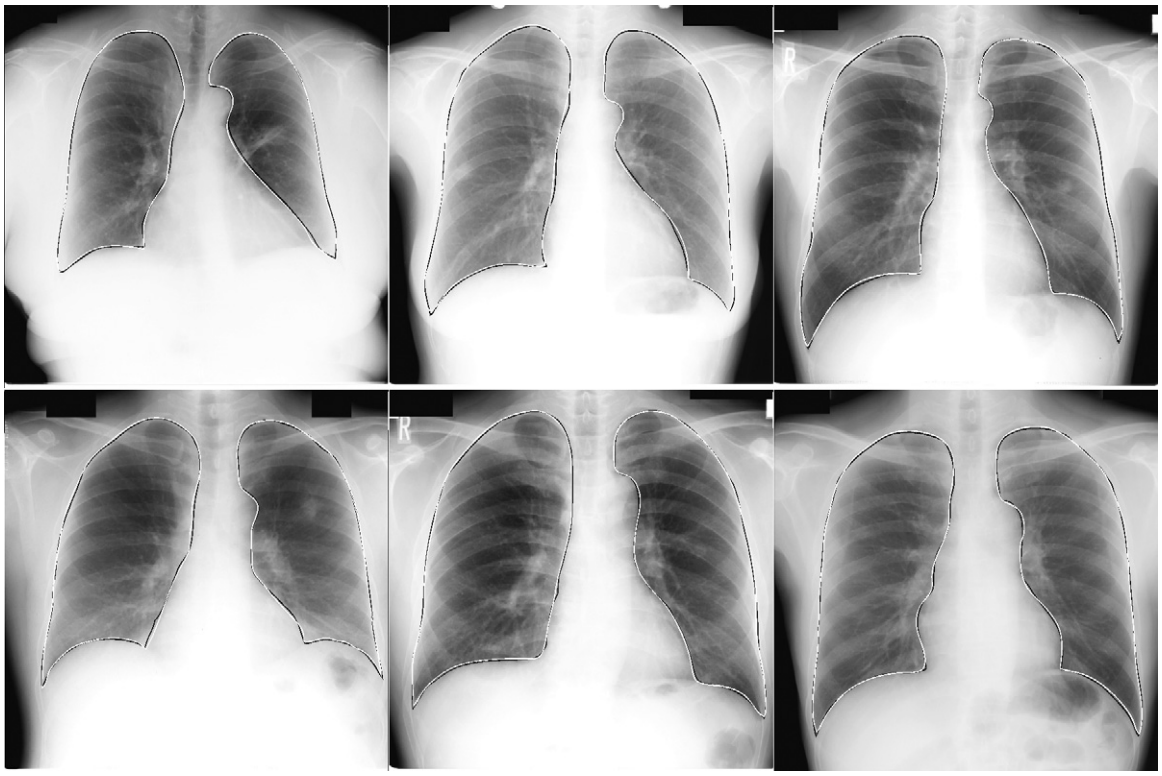

Fig. 6. Examples of segmentations in postero-anterior view form JSRT dataset. The computed boundary (white) is superimposed along with reference boundary (black).

5.1. Performances of segmentation process

The quality of the segmentation was first visually evaluated by an expert physician who was asked to judge the overall correctness of the outlined silhouette with respect to apexes, costophrenic angles and maximal-distance points. All images in JSRT were rated as correctly segmented. In EMPH, the images of 221 (out of 225) cases were retained correctly segmented. As shown in the panels

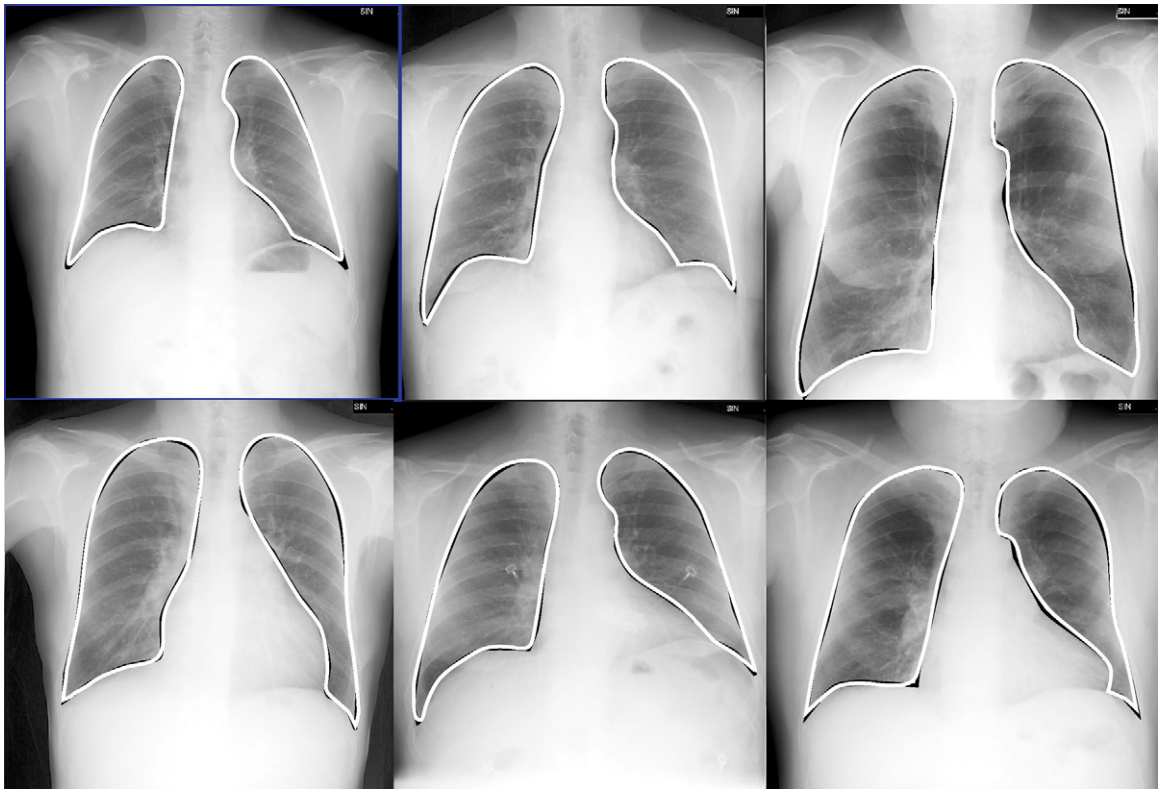

Fig. 7. Examples of segmentations in postero-anterior view form EMPH dataset: computed boundary (white) and reference boundary (black) are shown.

Please cite this article in press as: Coppini G, et al. A computer-aided diagnosis approach for emphysema recognition in chest radiography. Med Eng Phys (2012), http://dx.doi.org/10.1016/j.medengphy.2012.03.011

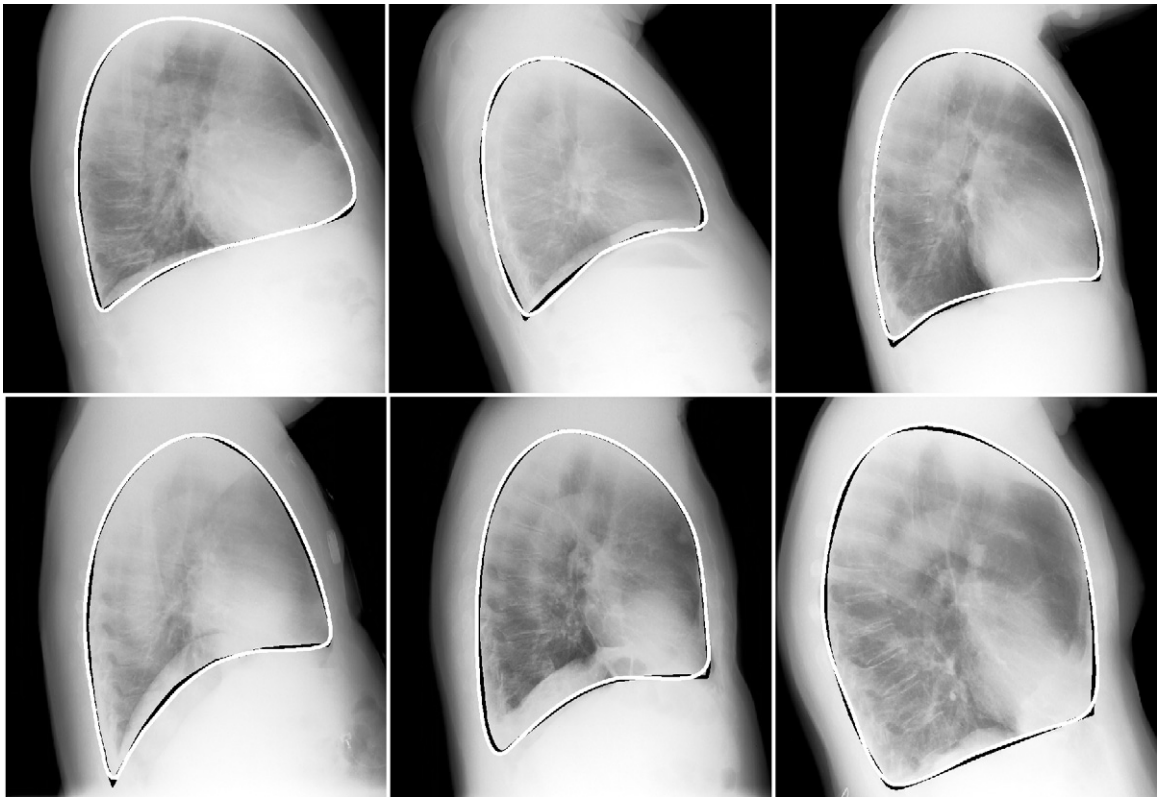

Fig. 8. Examples of segmentations in lateral view (EMPH dataset): computed boundary (white) and reference boundary (black) are shown.

of Fig. 9, segmentation failed in one postero-anterior radiogram and in three lateral radiographs. That was attributed to poor image contrast and the presence of anomalous radiographic patterns not related to emphysema.

A quantitative test assessed the behavior of the procedure by comparing the computer-recognized regions versus the corresponding ones traced by medical expert (as described in (2)). Let $\mathcal{R}_{ref}$ and $\mathcal{R}_{est}$ be the regions enclosed in the reference contour and in the estimated one. For each boundary we computed the True Positive area ($TP = |\mathcal{R}_{est} \cap \mathcal{R}_{ref}|$), False Negative ($FN = |\mathcal{R}_{est} - \mathcal{R}_{ref}|$) and False Positive ($FP = |\mathcal{R}_{ref} - \mathcal{R}_{est}|$) areas. Quality of segmentation was assessed by three commonly used metrics:

- Overlap percentage Ω (also known as Jaccard index):

$$\Omega = \frac{TP}{TP + FP + FN} = \frac{|\mathcal{R}_{est} \cap \mathcal{R}_{ref}|}{|\mathcal{R}_{est} \cup \mathcal{R}_{ref}|}$$

- Dice Similarity Coefficient (DSC):

$$DSC = \frac{|\mathcal{R}_{est} \cap \mathcal{R}_{ref}|}{|\mathcal{R}_{est} + \mathcal{R}_{ref}|}$$

It is worth mentioning that Ω and DSC are closely related. For a given region one has:

$$\Omega = \frac{DSC}{2 - DSC}.$$

- Average contour distance (ACD).

To evaluate ACD, for each point on the boundary of $\mathcal{R}_{est}$ the distance between its closest point on the contour of $\mathcal{R}_{ref}$ is first computed, distances are subsequently averaged over all points of $\mathcal{R}_{est}$ boundary. To symmetrize the measurement, the calculation is repeated by interchanging the two boundaries and the two distance values are averaged. ACD values are given in millimeters.

Table 1
Segmentation results for the JSRT dataset.

	Ω	DSC	ACD (mm)
Postero-anterior (total)	92.7 ± 3.3	95.5 ± 3.7	1.73 ± 0.87
Postero-anterior right	94.0 ± 3.1	96.5 ± 5.7	1.32 ± 0.89
Postero-anterior left	91.6 ± 2.5	94.5 ± 6.1	1.82 ± 0.92

In Table 1 we report the average values, expressed as mean plus/minus standard deviation, of Ω, DSC and ACD for JSRT dataset. Values for right and left profile respectively are also provided. In Table 2 corresponding values from EMPH dataset are given, including data for postero-anterior and lateral views (failed segmentations were not included in this analysis). Segmentation metrics are slightly, but seemingly not significantly, better in postero-anterior view.

5.2. Performances of emphysema classification

Classification of emphysema was assessed by Receiver Operating Characteristics (ROC) using EMPH dataset. Two different

Table 2
Segmentation results for the EMPH dataset.

	Ω	DSC	ACD (mm)
Postero-anterior (total)	93.1 ± 2.9	96.1 ± 3.5	1.62 ± 0.92
Postero-anterior right	95.7 ± 2.2	97.0 ± 4.1	1.02 ± 0.95
Postero-anterior left	92.2 ± 3.1	95.1 ± 6.2	1.86 ± 0.92
Lateral	94.5 ± 4.6	91.0 ± 6.3	2.22 ± 0.86

Please cite this article in press as: Coppini G, et al. A computer-aided diagnosis approach for emphysema recognition in chest radiography. Med Eng Phys (2012), http://dx.doi.org/10.1016/j.medengphy.2012.03.011

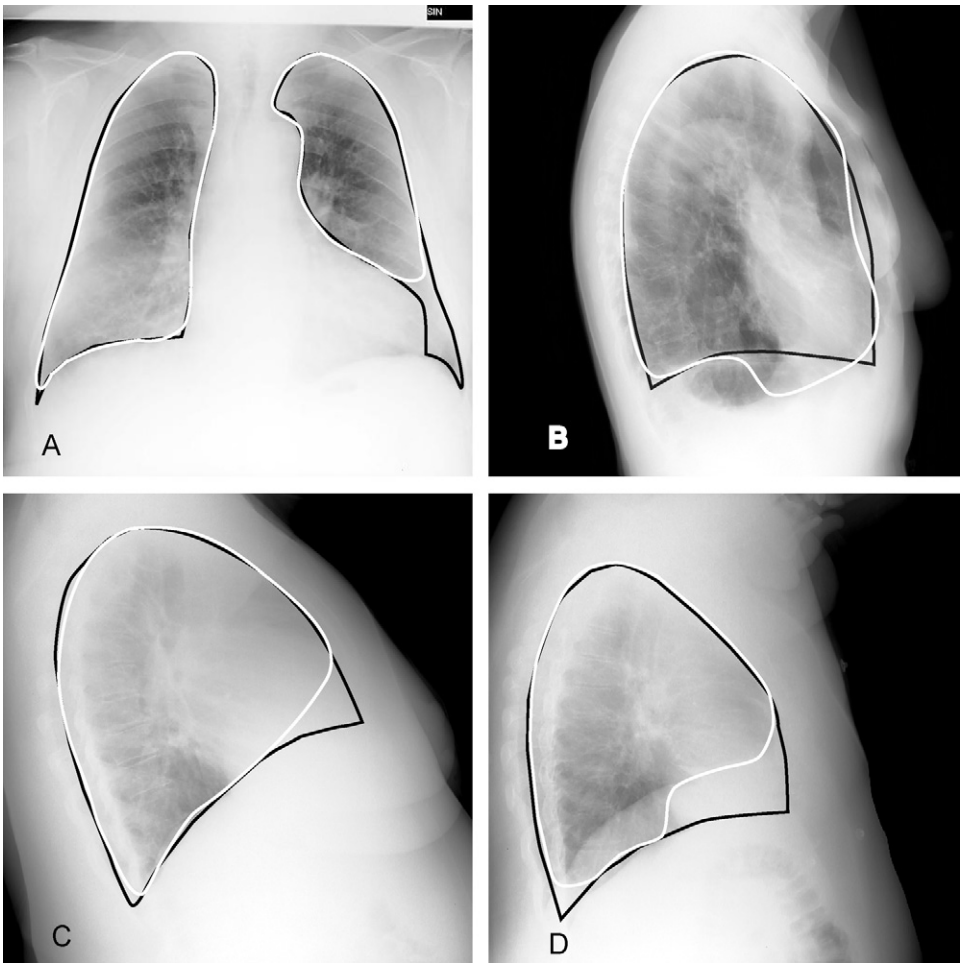

Fig. 9. Images of EMPH whose segmentation were rated as failed by an expert physician. Images in panels A, C, D are from non-emphysematous cases, panel B is from an emphysematous patient; computed boundary (white) and reference boundary (black) are shown.

tests were performed: (i) emphysema recognition using manual segmentation and (ii) emphysema recognition with automatic segmentation.

The plot on the left panel of Fig. 10 is obtained from all the cases in EMPH using the hand-traced contours. The area under the curve (AUC) was 0.976 (95% CI: 0.967–0.997). Confidence intervals were estimated by bootstrap [30].

These results are very close to those obtained by automatic segmentation that are shown in right panel of Fig. 10. In this test, cases with failed segmentations (3 non-emphysema cases and 1 emphysema case) were excluded, obtaining e subset of EMPH with 221 cases (91 with emphysema and 130 with no emphysema). The area under the curve was 0.968 (95% CI, 0.959–0.998).

In Table 3, true positives, true negatives, false positives and false negatives are provided along with sensitivity, specificity and accuracy for a cutoff $p_{TH} = 0.55$. The values are valid both for manual and for automatic segmentation. It is worth noting that failures in recognizing emphysema occurred in five cases with mild or trace emphysema, their score at CT being less or equal than 15. The false positive cases had a computed emphysema probability from 0.56 to 0.59.

To evaluate the effect of shape alteration not related to emphysema, images were retrospectively analyzed by an expert physician for the presence of skeletal distortions. Forty-four patients showed signs of kyphosis, rated as mild in thirty-five and moderate in nine. No misclassification was observed in these patients.

Table 3
Classification results using the cutoff $p_{TH} = 0.55$. Values were computed from the subset of EMPH of correctly segmented images (221 cases, 91 with emphysema and 130 with no emphysema). The same results were obtained using manual segmentation.

TP	TN	FP	FN	Sensitivity	Specificity	Accuracy
86 (91)	125 (130)	5	5	94.5%	96.1%	95.4%

6. Discussion

A computational approach to diagnose emphysema from digital chest radiographs was described. It is based on the analysis of the shape of lung silhouette which is altered by chronic hyperinflation. The resulting system includes two main processes: (i) automatic segmentation of the lung fields exploiting image features and prior knowledge by means of a fuzzy boundary model coupled to neural-network processing; (ii) emphysema recognition by a dedicated shape descriptor and a neural-network classifier.

As to the segmentation process, in a vast majority of cases the computed contours were adequate for a correct classification. That was also confirmed both by visual inspection and comparison of computed contours with hand-traced ones. Measurements on JSRT public dataset suggest that our method performs, in segmenting postero-anterior view, at least as well as ASM/AAM methods [23,24].

Segmentation of the lateral view, even though with slightly inferior metrics with respect to postero-anterior projection, resulted

Please cite this article in press as: Coppini G, et al. A computer-aided diagnosis approach for emphysema recognition in chest radiography. Med Eng Phys (2012), http://dx.doi.org/10.1016/j.medengphy.2012.03.011

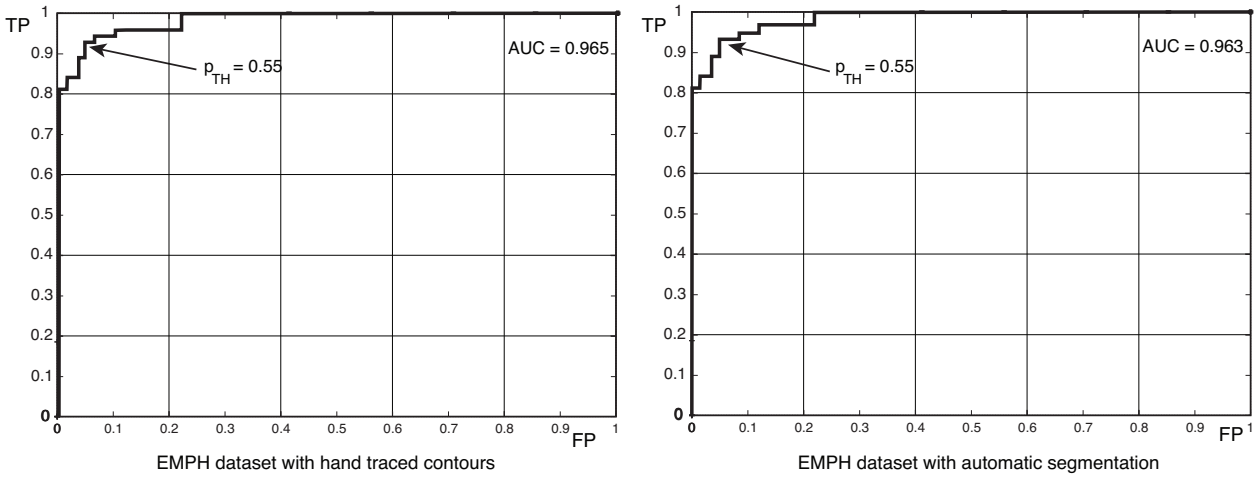

Fig. 10. Left panel: the ROC curve obtained using hand-traced contours from all the images in EMPH dataset, right panel: the ROC curve obtained from automatically segmented images in EMPH (excluding failed segmentations).

well suited for emphysema recognition. In general, the boundary of the lung fields was properly recognized allowing confident detection of the needed feature points that include costophrenic angles, lung apex, and maximum-distance points used to define the triangles. We observed a few segmentation failures that are mainly related to poor image quality or to distortion of lung silhouette as, for example, in the presence of a raised hemidiaphragm. For the sake of this work, wrongly segmented cases were withdrawn from the classification test. In routine implementation of the system, such failures could be dealt with a minimal editing of the computed contour. It is worth noting that the availability of lung boundary in postero-anterior and lateral views may be usefully exploited to compute additional parameters such as the radiographic total lung capacity [31].

As to shape description and classification, the described system exhibits improved recognition capabilities in comparison with previous works [8,10]. In particular, the adopted shape-descriptor was able to successfully cope with alterations of lung silhouette not related to the presence of emphysema, such as skeletal distortions. In the present study, we found no significant difference between manual ad automatic segmentation. The area under the ROC curve was 0.976 for manual segmentation and 0.968 for the automatic one, respectively. At the selected probability cut-off (p_{TH} =0.55), the sensitivity reached 94.5% and the specificity 96.1%, with an overall accuracy of 95.4%.

7. Conclusion

In summary, we describe an automatic system that allows the recognition of emphysema on two-sided digital chest radiographs. The system could be advantageously used in clinical practice as it is simple, inexpensive, and requires no special expertise. Its application may cut down the costs of the diagnostic procedures for emphysema and minimize the radiation to the patient.

Conflict of interest

All the authors declare that no actual or potential conflict of interest in relation to this article exists.

References

[1] Ciba Guest Symposium Report. Terminology, definitions, and classification of chronic pulmonary emphysema and related conditions. Thorax 1959;14:286–99.
[2] Pratt PC. Role of conventional chest radiography in diagnosis and exclusion of emphysema. Am J Med 1987;82:998–1006.
[3] Thurlbeck WM, Müller NL. Emphysema: definition, imaging, and quantification. Am J Roentgenol 1994;163:1017–25.
[4] Sluimer I, Schilham A, Prokop M, van Ginneken B. Computer analysis of computed tomography scans of the lung: a survey. IEEE Trans Med Imaging 2006;25:385–405.
[5] Sutinen S, Christoforidis AJ, Klugh GA, Pratt PC. Roentgenologic criteria for the recognition of nonsymptomatic pulmonary emphysema. correlation between roentgenologic findings and pulmonary pathology. Am Rev Respir Dis 1965;91:69–76.
[6] Schaefer-Prokop C. Plain chest radiography: the digital revolution. Eur Respir Monit 2004;30:23–38.
[7] Miniati M, Monti S, Stolk J, Mirarchi G, Falaschi F, Rabinovich R, et al. Value of chest radiography in phenotyping chronic obstructive pulmonary disease. Eur Respir J 2008;31:509–14.
[8] Coppini G, Miniati M, Paterni M, Monti S, Ferdeghini EM. Computer-aided diagnosis of emphysema in COPD patients: neural-network-based analysis of lung shape in digital chest radiographs. Med Eng Phys 2007;29:78–86.
[9] van Ginneken B, Hogeweg L, Prokop M. Computer-aided diagnosis in chest radiography: beyond nodules. Eur J Radiol 2009;72:226–30.
[10] Miniati M, Coppini G, Monti S, Bottai M, Paterni M, Ferdeghini EM. Computer-aided recognition of emphysema on digital chest radiography. Eur J Radiol 2011;80:e169–75.
[11] Li L, Zheng Kallergi YM, Clark RA. Improved method for automatic identification of lung regions on chest radiographs. Acad Radiol 2001;8:629–38.
[12] Armato SGML, Giger K, MacMahon H. Automated lung segmentation in digitized posteroanterior chest radiographs. Acad Radiol 1998;5:245–55.
[13] Xu XW, Doi K. Image feature analysis for computer-aided diagnosis: accurate determination of ribcage boundary in chest radiographs. Med Phys 1995;22:617–26.
[14] Xu XW, Doi K. Image feature analysis for computer-aided diagnosis: detection of right and left hemidiaphragm edges and delineation of lung field in chest radiographs. Med Phys 1996;23:1613–24.
[15] Duryea J, Boone JM. A fully automatic algorithm for the segmentation of lung fields in digital chest radiographic images. Med Phys 1995;22:183–91.
[16] Brown MS, Wilson LS, Doust BD, Gill RW, Sun C. Knowledge-based method for segmentation and analysis of lung boundaries in chest X-rays images. Comput Med Imaging Graph 1998;22:463–77.
[17] McNitt-Gray M, Huang H, Sayre J. Feature selection in the pattern classification problem of digital chest radiograph segmentation. IEEE Trans Med Imaging 1995;14:537–47.
[18] Tsujii O, Freedman MT, Mun SK. Automated segmentation of anatomic regions in chest radiographs using an adaptive-sized hybrid neural network. Med Phys 1998;6:998–1007.
[19] Vittitoe NF, Vargas-Voracek R, Floyd Jr CE. Identification of lung regions in chest radiographs using markov random field modeling. Med Phys 1998;6:976–85.
[20] Hasegawa A, Lo SB, Lin JS, Freedman MT, Mun SK. A shift-invariant neural network for the lung field segmentation in chest radiography. J VLSI Signal Proc 1998;18:241–50.
[21] van Ginneken B, ter Haar Romeny BM. Automatic segmentation of lung fields in chest radiographs. Med Phys 2000;10:2445–55.
[22] van Ginneken B, Frangi A, Staal J, ter Haar Romeny B, Viergever M. Active shape model segmentation with optimal features. IEEE Trans Med Imaging 2002;21:924–33.
[23] van Ginneken B, Stegmann MB, Loog M. Segmentation of anatomical structures in chest radiographs using supervised methods: a comparative study on a public database. Med Image Anal 2006;10:19–40.

Please cite this article in press as: Coppini G, et al. A computer-aided diagnosis approach for emphysema recognition in chest radiography. Med Eng Phys (2012), http://dx.doi.org/10.1016/j.medengphy.2012.03.011

[24] Shi Yonghong, Qi Feihu, Xue Zhong, Chen Liya, Ito K, Matsuo H, et al. Segmenting lung fields in serial chest radiographs using both population-based and patient-specific shape statistics. IEEE Trans Med Imaging 2008;27: 481–94.
[25] Shiraishi J, Katsuragawa S, Ikezoe J, Matsumoto T, Kobayashi T, Komatsu K, et al. Development of a digital image database for chest radiographs with and without a lung nodule: receiver operating characteristic analysis of radiologists detection of pulmonary nodules. Am J Roentgenol 2000;174: 71–4.
[26] Armato SG, Giger ML, Ashizawa K, MacMahon H. Automated lung segmentation in digital lateral chest radiographs. Med Phys 1998;25: 1507–20.
[27] Carrascal FM, Carreira JM, Souto M, Tahoces PG, Gómez L, Vidal JJ. Automatic calculation of total lung capacity from automatically traced lung boundaries in postero-anterior and lateral digital chest radiographs. Med Phys 1998;25:1118–31.
[28] Kohonen T. Self-Organizing Maps. Springer: Berlin; 2001.
[29] Bishop CM. Neural Networks for Pattern Recognition. New York: Oxford University Press; 1995.
[30] Obuchowski NA, Lieber ML. Confidence intervals for the receiver operating characteristic area in studies with small samples. Acad Radiol 1998;5:561–71.
[31] Harris TR, Pratt PC, Kilburn KH. Total lung capacity measured by roentgenograms. Am J Med 1971.

Please cite this article in press as: Coppini G, et al. A computer-aided diagnosis approach for emphysema recognition in chest radiography. Med Eng Phys (2012), http://dx.doi.org/10.1016/j.medengphy.2012.03.011